

Efficient adsorptive removal of industrial dye from aqueous solution by synthesized zeolitic imidazolate framework-8 loaded date seed activated carbon and statistical physics modeling

Gamil A.A. Al-Hazmi^{a,b}, Mohamed A. El-Bindary^c, Mohamed G. El-Desouky^d, Ashraf A. El-Bindary^{e,*}

^aChemistry Department, Faculty of Science, King Khalid University, P.O. Box 9004, Abha, Saudi Arabia, email: jmarshd@kku.edu.sa (orcid.org/0000-0001-7352-4831)

^bChemistry Department, Faculty of Applied Sciences, Taiz University, Taiz 82, Yemen

^cBasic Science Department, Higher Institute of Engineering and Technology, New Damietta 34517, Egypt, email: abindary@yahoo.com (orcid.org/0000-0001-5977-1465)

^dEgyptian propylene and polypropylene company, Port Said, Egypt, email: ch.moh.gamal@gmail.com (orcid.org/0000-0001-6060-463X)

^eChemistry Department, Faculty of Science, Damietta University, Damietta, Egypt, email: abindary@du.edu.eg/abindary@yahoo.com (orcid.org/0000-0002-4494-3436)

Received 12 December 2021; Accepted 9 March 2022

ABSTRACT

New adsorbents of DSAC@ZIF-8 (0.05:0.6) and DSAC@ZIF-8 (0.05:0.6) were prepared using date seed activated carbon (DSAC) loaded at zeolitic imidazolate framework-8 (ZIF-8). The obtained adsorbents DSAC@ZIF-8 (0.05:0.6) and DSAC@ZIF-8 (0.1:0.6) were characterized by Fourier-transform infrared spectroscopy, scanning electron microscopy, powder X-ray diffraction, nitrogen adsorption/desorption tests at 77 K revealed the surface area to be 460.23 m²/g for DSAC@ZIF-8 (0.1:0.6). This material showed a high affinity for Gentian violet (GV) uptake from aqueous solutions: the maximum sorption capacity reached 638.99 mg/g at pH 9.0 and ambient temperature. Uptake kinetics and sorption isotherms were obtained and modelled using conventional and simple equations: the best results were respectively obtained with the pseudo-second-order rate equation and the Langmuir equation. The activation energy of absorption also was measured to be 15.87 kJ/mol, showing that the process of chemisorption is included. The distribution coefficient was obtained at different temperatures and the thermodynamic parameters have been calculated: the sorption is endothermic, spontaneous (especially at high relative temperature), and contributes to increasing the entropy (randomness) of the system. HCl (1.0 M) was used for GV desorption from DSAC@ZIF-8, and the sorbent could be efficiently recycled for a minimum of three sorption/desorption cycles. Therefore, sorbent could serve as a promising adsorbent for GV removal from industrial wastewater.

Keywords: DSAC@ZIF-8; Adsorption isotherm; Thermodynamics, Gentian violet; Statistical physics modeling

* Corresponding author.

1. Introduction

One of its world's most difficult environmental problems involves effluents, and it requires immediate attention. Human and industrial wastes are best disposed of in the marine environment. The latter has resulted in increased pollution, posing a hazard to the environment as well as human health. Water impurities come in a variety of forms, containing gases, inorganic dissolved substances, organic solutes, suspending components, and microbes being among the most common. Even though most of them can be removed using standard procedures, the concentration of harmful compounds left in the water after treatment can sometimes exceed the permissible level. The majority of them are organic substances, including dyes, that are emitted with the textile business produces massive volumes besides cause toxicity, odor, disagreeable taste, and watercolor, resulting in water quality degradation and the extinction of aquatic life. As a result, treating colored effluents before they are discharged into the environment is critical. The production and usage of dyeing textiles with synthetic colors is now a lucrative industry; Every year, nearly 700,000 tons of colors were manufactured around the world. About 20% of this amount is industrial trash that has not been treated before being loaded. Environmentalists, on the other hand, are concerned about their use. Because synthetic dyes contain sulfur, colors, lead, and mercury including copper, arsenic, and lead, as well as nitrates, acetic acid, surfactants, enzymes, and chromium complexes, they are very poisonous to all kinds of life [1–3].

Cadmium, mercury, nickel, cobalt, and a few other chemicals are used in this process are some of the metals used [4,5]. Nylon is used printing inks and also a dermatological stain a veterinary medicine agent. Gentian violet (GV) is toxic and can cause death cause irritation when skin absorption, as well as inhalation and ingestion [5,6]. It might lead to renal failure and inflammation of the eyes which can result in irreversible blindness in severe cases. As a result, removing GV from the effluent is quite important [7,8]. Some of these approaches are effective, but they have drawbacks, such as excessive chemical use, the formation of concentrated sludge, which poses major disposal issues, and the absence of effective color reduction.

Among the above-mentioned methods, batch adsorption is considered a promising method because of its simple operation and low cost. Besides, advanced oxidation based on peroxymonosulfate (PMS) activation has shown potential in the removal of organic pollutants in recent years. Developing adsorbent or catalyst materials with low cost, high efficiency and environmental performances are crucial for both processes [9]. Although a large number of materials has been developed for adsorption or catalytic degradation, activated carbon (AC) is still, one of the most common materials owing to its large surface area, low cost, and easy availability. However, the as-prepared AC often has a low capacity and selectivity for adsorption and weak catalytic activity for advanced oxidation. Thus, different surface modification methods were used to improve the performance of AC, such as treatment by acid, base or oxidation, and metal oxides impregnation. Among those strategies, the impregnation

of AC with metals is gaining wide interest in virtue of the significantly enhanced performances. However, the impregnation of metal often leads to an occlusion of its pores, which significantly reduces the surface area and pore volume and consequently affects the improvement of its performance [10,11].

Metal-organic frameworks (MOFs) are porosity crystallographic frameworks made up of ionic species (or groups) and organic linkers. MOFs have sparked global attention and have been employed in a variety of sectors, including separating of gases/recycling, power storage, adsorbent materials, and catalysts because of their exceptional. MOFs are being used for adsorption and disposal of hazardous waste as for water-based solutions is becoming more common these days, there seem to be goals for both various inorganic contaminants. Hydrophobic interactions, electrostatic enhancements, and interrelations are all involved in the adsorption of pollutants on MOFs. Because of their high porosity, MOFs have previously been reported to be promising in the capture of certain dyes at water systems because of considerable surface heterogeneity and significant electrostatic forces [12].

However, for water treatment, the nano-sized MOF-derived carbons often suffer from drawbacks like being difficult to be separated from water and high cost. The zeolitic imidazolate framework-8 (ZIF-8) modified with date seed activated carbon (DSAC) was characterized using Fourier-transform infrared spectroscopy (FTIR), X-ray diffraction (XRD), scanning electron microscopy (SEM), energy-dispersive X-ray spectroscopy (EDX) and N₂ adsorption-desorption and used as adsorbent for removal of GV from water. The results show that ZIF-8 modified with DSAC (DSAC@ZIF-8) exhibits high adsorption capacity as adsorbent long-term stability and easy recovery in removing GV from water. The adsorption isotherms also were examined. Modeling accomplished using models that are well known to test the efficiency of DSAC@ZIF-8 on dye adsorptions, equilibrium, kinetic, and thermodynamic studies were employed.

2. Materials and methods

2.1. Chemicals

Chemicals were utilized in their natural state, with no further processing. They consist of zinc nitrate hexahydrate, 2-methylimidazole (Hmim), ammonium hydroxide solution (Sinopharm Chemical Reagent Co., Ltd., China). Date seeds were collected from a marketplace, and GV was bought from Merck KGaA, Darmstadt, Germany, 64271.

2.2. Preparation of adsorbent

The adsorbent will be synthesized at several steps as the following:

2.2.1. Synthesis of activated carbon from date seeds

As a preliminary, date seeds were gathered. The seeds were washed several rinsed with deionized water before even being dried at 110°F for 24 h. The dried seeds were

crushed and processed in an electric grinder before being sieved in via a 300 m screen. The finely ground date seed grains were mixed with KOH in a 1:1 weight ratio and then carbonized for 3 h at 700°C in a furnace with a nitrogen flow of 120 mL/min. After cooling to ambient temperature collect it in a clean tube [13].

2.2.2. Preparation of zeolitic imidazolate framework-8

ZIF-8 has been synthesized according to previously published reports [14]. At standard synthesis, 2.97 g of zinc nitrate hexahydrate was dissolved in 3 g of deionized water. The zinc nitrate and Hmim solutions were mixed after 1.64 g of Hmim was introduced to 20.75 mL of ammonium hydroxide solution. Instantly, the solution developed a milk-like suspension, and it was agitated for 10 min at room temperature to conclude crystallization. The sample was collected by centrifuge and rinsed three times with deionized water until the pH of the final product was around 7, after which it was dried overnight at 60°C.

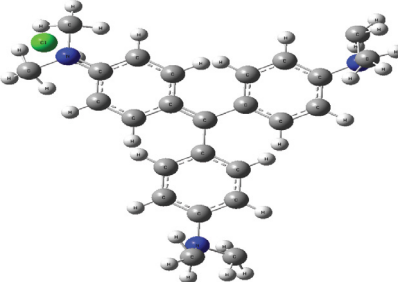
2.2.3. Preparation of DSAC@ZIF-8

Solution A: trial 0.05:0.6 (Hexahydrate zinc nitrate, 2 mmol, 0.6 g) and 0.05 g DSAC and trial 0.1:0.6 (Hexahydrate zinc nitrate, 2 mmol, 0.6 g) and 0.1 g DSAC were dissolved as in 7.5 mL of methanol. Solution B: (2-methylimidazole, 8 mmol, 0.65 g) was also dissolved in 7.5 mL of methanol. Add (solution A) dropwise over (solution B) with ultrasonic treatment for several 2 h at 60°C; the powder obtained was collected by centrifugation and dried at oven overnight. The brown crystals of DSAC@ZIF-8 (0.05:0.6) and DSAC@ZIF-8 (0.1:0.6) crystals have been obtained here [15].

2.3. Adsorbate preparation

Gentian violet (GV) solution (1×10^{-3} mol/L) was prepared by dissolving a suitable amount as required concentration. The levels obtained from standard stock solution were in the range of (8×10^{-5} to 1×10^{-3} mol/L) [16]. The GV solution, including the others of the experiment, were made with deionized water. During the initial pH adjustments, HCl (0.1 M) and NaOH (0.1 M) were used to modify the pH of the solution (Table 1).

Table 1
Properties of the adsorbate GV

Dye	Molecular formula	Ball and stick model of dye	Molar mass (g/mol)	λ_{\max}	Electrical property
GV	$C_{25}H_{30}N_3Cl$		407.99	590	Cationic

2.4. Characterization of DSAC@ZIF-8

FTIR spectra (KBr discs, 4,000–400 cm^{-1}) by Jasco 4100 spectrophotometer. The structural differences of the as-prepared DSAC@ZIF-8 were investigated using the X-ray diffraction (XRD) method. The powder XRD patterns were captured using a Siemens D500 X-ray diffractometer equipped with a Cu Ka source of radiation. UV-visible spectra from a Perkin Elmer AAnalyst 800 spectrophotometer Model AAS with a 1.0 cm model system. The pH meter utilized was a WTW 720 model digital pH meter. The adsorption/desorption isotherm of N_2 on adsorbent at $P/P_0 = 6.58 \times 10^{-5}$ torr and 77 K was performed with a Quantachrome TouchWin Instruments version 1.11. HANNA instrument pH meter (model 211) was used for pH modification. Scanning electron microscopy (JEOL, JSM7600F, Japan) was used to examine the microstructure of DSAC@ZIF-8. The specimen was then deposited onto a copper substrate after being sputter-coated with a homogenous gold layer. EDX was used to analyze the elemental distribution of DSAC@ZIF-8 on a Leo1430VP microscope with a 5 kV operating voltage.

2.5. Batch adsorption experiments: experimental design

Batch adsorption studies were carried out by shaking 50 mL conical flasks containing 0.02 g of (DSAC@ZIF-8) and 25 mL of GV solutions of desired concentration range from 2.76×10^{-4} to 2.2×10^{-3} mol/L with adjusted pH on an orbital shaker machine at 200 rpm at 25°C. The solution pH was adjusted with 0.1 M HCl and 0.1 M NaOH solutions. At the end of the adsorption period, the supernatant solution was separated by a centrifuge. Then the concentration of the residual dye was determined UV-Vis spectrophotometer spectrophotometrically by monitoring the absorbance at 407.99 nm for GV and the adsorption capacity q_e (mg/g) and the dye removal rate (%) were calculated using the formulas:

$$\%R = \frac{(C_0 - C_t)}{C_0} \times 100 \quad (1)$$

$$q_e = \frac{(C_0 - C_e)V}{M} \quad (2)$$

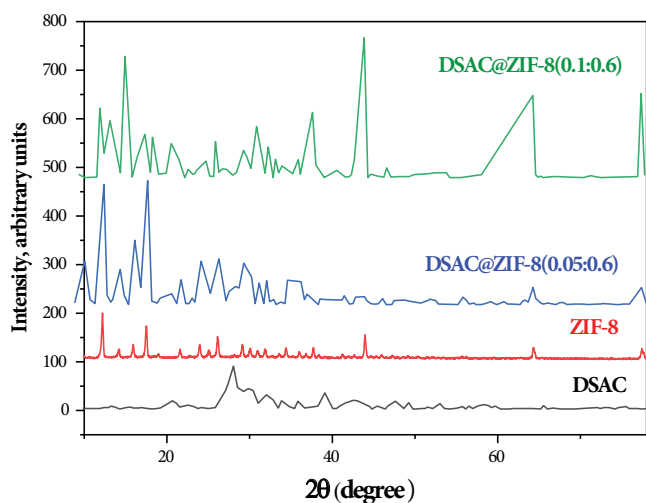


Fig. 1. X-ray diffraction pattern of DSAC, ZIF-8, DSAC@ZIF-8 (0.05:0.6), and ZIF-8 (0.1:0.6).

where C_0 (mg/L) and C_e (mg/L) are the dye solution's initial concentration and equilibrium concentration, respectively. V (mL) is the starting volume; m (g) is the mass of the adsorption equilibrium the amount of adsorbent to use the characteristics of the experiment that were associated to the influencing factors:

3. Results and discussion

3.1. Characterization of DSAC@ZIF-8

3.1.1. X-ray diffraction patterns

The XRD patterns of the DSAC, ZIF-8, as-prepared DSAC@ZIF-8 (0.05:0.6) and DSAC@ZIF-8 (0.1:0.6) are shown in Fig. 1. One broad peak for activated carbon from date seeds may be found on the XRD graph between angles (2θ) of 25° and 27° where the broad peaks in the XRD pattern indicate that the activated carbon is amorphous, whereas sharp peaks indicate that it is crystalline at synthesized ZIF-8 (JCPDS 00-062-1030) [17,18]. The broad peak increases as the calcination temperature rise. After mixing ZIF-8 with DSAC with the different ratios as mentioned above several new peaks appear, indicating that ZIF-8 was loaded onto DSAC successfully. The sharp diffraction of ZIF-8 is decreased in composites of DSAC@ZIF-8 (0.1:0.6) especially at angles (2θ) 58° and 65° . This is an excellent adsorption characteristic of adsorbents.

3.1.2. Fourier-transform infrared analysis

Functional groups present at materials of ZIF-8, DSAC@ZIF-8 (0.05:0.6), and DSAC@ZIF-8 (0.1:0.6), FTIR measurements between $4,000$ and 400 cm^{-1} . Bands of absorption at $3,444\text{ cm}^{-1}$ for the O–H strain were considerably varied implying that a hydrogen bond will be formed during GV adsorption. The $\text{C}=\text{O}$ There are two bands at $1,015$ and 921 cm^{-1} that correlate to $(\text{C}-\text{H})$ alkyl halide and aromatic, respectively, and also bands at $1,636\text{ cm}^{-1}$ (carboxyl) and $1,396\text{ cm}^{-1}$ (carbonyl) (Fig. 2) [19–22].

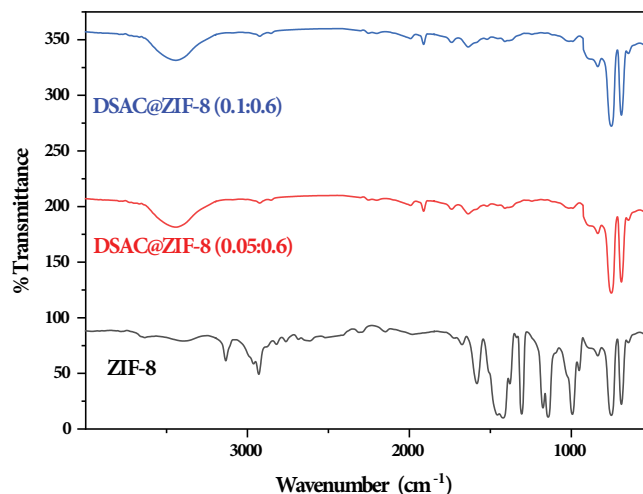


Fig. 2. FTIR spectrum of DSAC@ZIF-8 (0.05:0.6) and DSAC@ZIF-8 (0.1:0.6).

3.1.3. Brunauer–Emmett–Teller surface area

The adsorption isotherm is classified as type III, DSAC@ZIF-8 (0.1:0.6), which is a type III isotherm. A hysteresis loop is observed at a larger relative pressure ($P/P_0 > 0.9$) due to the presence of pores that are generally microporous, with the surface staying almost entirely within the microspores, leaving little or no exterior surface for additional adsorption once loaded by adsorbate. The Brunauer–Emmett–Teller (BET) surface area for DSAC@ZIF-8 (0.1:0.6) was $460.23\text{ m}^2/\text{g}$ using a value of 16.2 for the N_2 molecule's cross-sectional area. The entire pore volume at operating pressure, on the other hand, the average pore diameter is 47.23 nm , and the capacity of the liquid is $5.48\text{ cm}^3/\text{g}$. DSAC@ZIF-8 (0.1:0.6) was classed as mesoporous by IUPAC because its pore size was 47.23 nm (between 2 to 50 nm) [23–26]. Also limitation absorption at high initial P/P_0 owing to the presence of a hysteresis loop H_3 , capillary condensation in a mesoporous media, and the presence of a hysteresis loop H_3 . Mono-multilayer adsorption is represented by the first loop, whereas desorption is represented by the second loop (Fig. 3).

3.1.4. SEM analysis

SEM has been considered a primary tool for characterizing the surface, fundamental physical properties, and morphology of the adsorbent surface. It is useful for defining the porosity, particle shape, and appropriate size spreading of the adsorbent. DSAC, ZIF-8 and DSAC@ZIF-8 (0.1:0.6) study were used to carry it out (Fig. 4). Because the mean diameter of DSAC@ZIF-8 (0.1:0.6) was between 165 and 348 nm , SEM examination confirmed that it was nanoparticles. DSAC@ZIF-8 (0.1:0.6) has a large number of pores where dyes have a strong chance of being adsorbed and trapped [16,27].

3.1.5. Energy-dispersive X-ray spectroscopy

The element composition in ZIF-8, DSAC, and DSAC@ZIF-8 (0.1:0.6) was evaluated using an EDX instrument

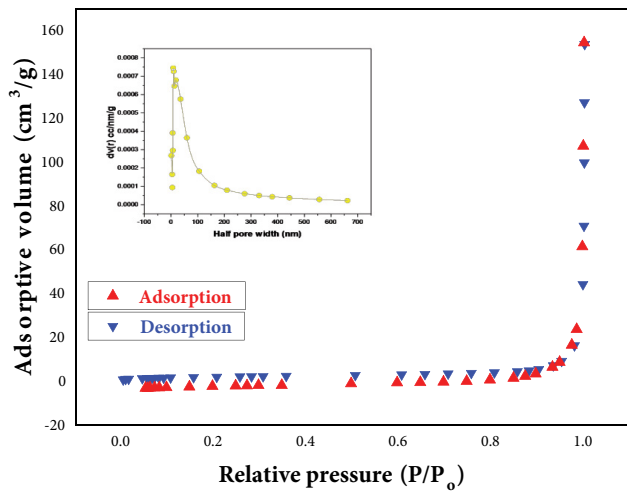


Fig. 3. DSAC@ZIF-8 (0.1:0.6) isotherm curve for N_2 adsorption/desorption.

(Fig. 5), and the results are presented in Table 2 as a percentage.

3.1.6. Determination of point of zero charge (pH_{PZC})

pH was one of the most important parameters for (GV) sorption, as it determined which ionic species were present in the adsorbate solution and the surface charge of the sorbent. The surface charge of the DSAC@ZIF-8 (0.1:0.6) was determined by the PZC, which is defined as the pH (pH_{PZC}) at which the positive charges on the surface equal the negative charges. The pH_{PZC} of DSAC@ZIF-8 (0.1:0.6) was found to be 7.4 (Fig. 6). This shows that below this pH, the DSAC@ZIF-8 (0.1:0.6) acquires a positive charge due to the protonation of functional groups and above this pH, a negative charge exists on the surface of DSAC@ZIF-8 (0.1:0.6). The adsorption of cationic dyes is favored at $pH > pH_{PZC}$ where the surface becomes negatively charged [16].

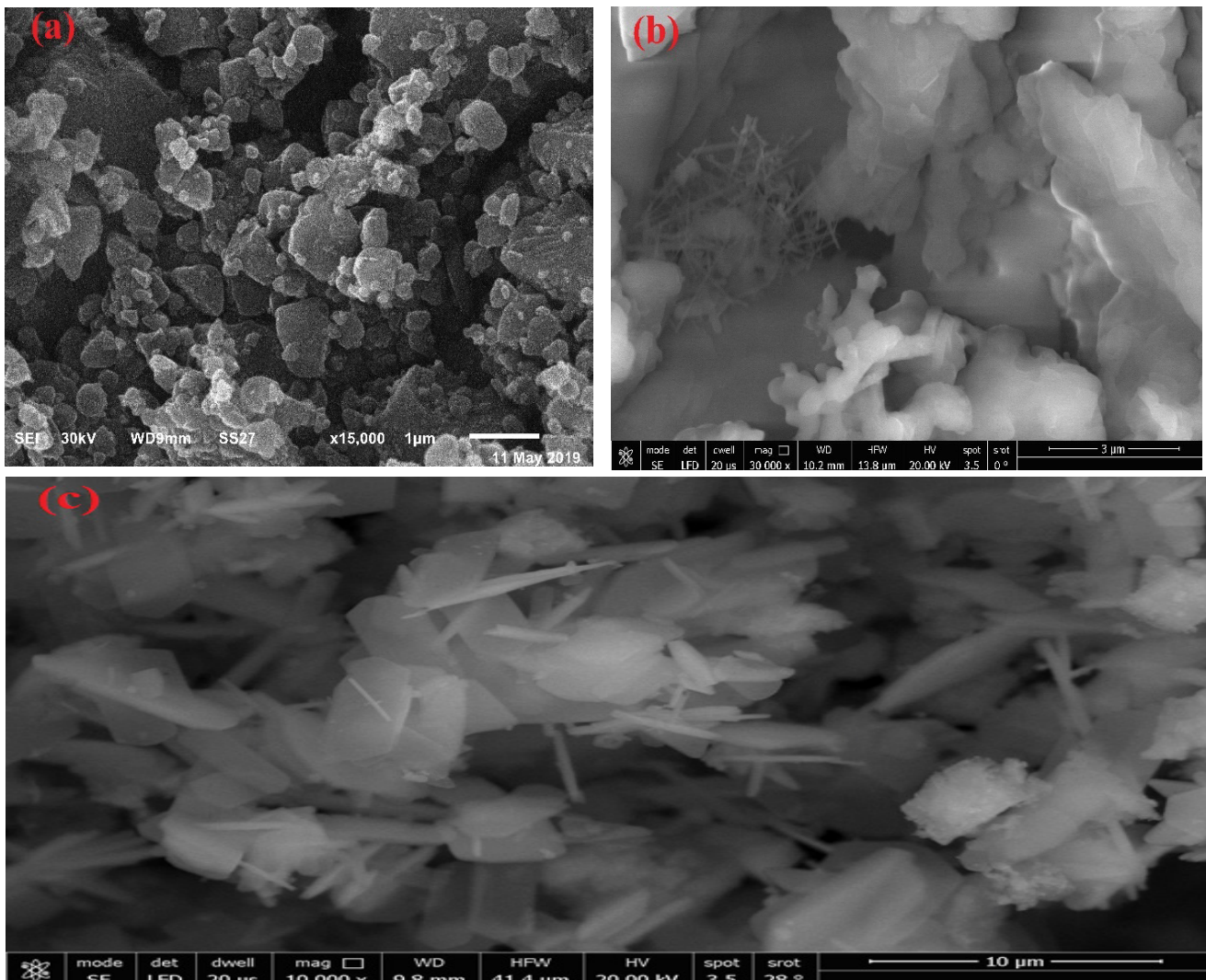


Fig. 4. SEM image (a) ZIF-8, (b) DSAC and (c) DSAC@ZIF-8 (0.1:0.6).

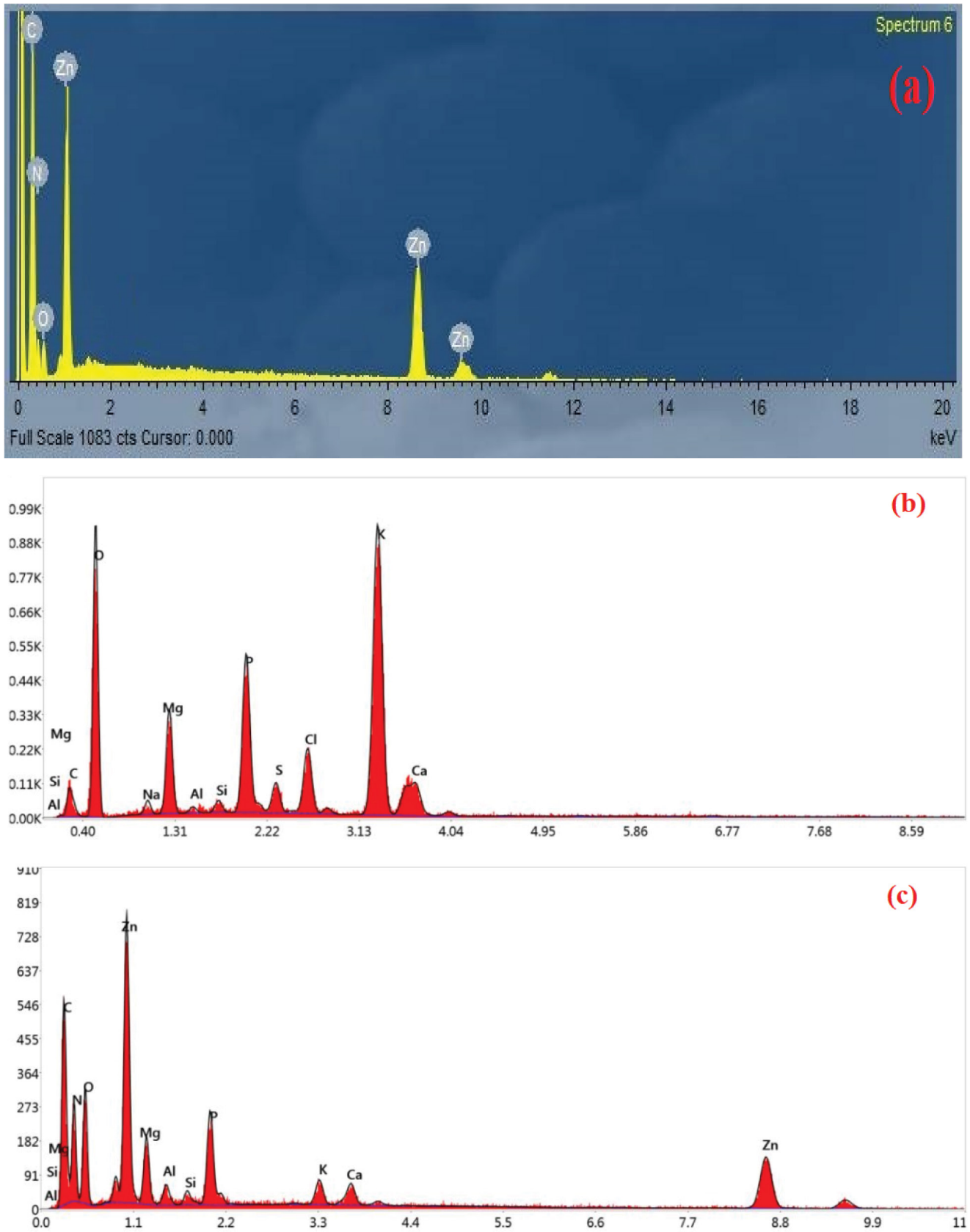


Fig. 5. EDX spectrum of (a) ZIF-8, (b) DSAC and (c) DSAC@ZIF-8 (0.1:0.6).

Table 2
The percent component in the structure ZIF-8, DSAC and DSAC@ZIF-8 (0.1:0.6)

Element	ZIF-8 weight %	DSAC weight %	DSAC@ZIF-8 (0.1:0.6) weight %
C	38.11	3.86	39.92
N	32.11	–	30.02
O	14.60	65.73	20.22
Zn	15.17	–	4.62
Mg	–	5.2	1.91
Al	–	0.2	0.12
Si	–	0.3	0.21
P	–	5.82	1.87
K	–	1.29	0.54
Ca	–	1.98	0.56
Na	–	1.16	–
Cl	–	2	–

3.2. Batch experiments

3.2.1. Effect of pH

In the acidic situation, the measurement that can be applied for GV dye has achieved its maximum, as shown in Fig. 7. When the pH level reaches 9, the adsorption capability decreases when the pH changes from 3 to 8. The effect of pH on adsorption performance may be connected to parameters like the ionic group and charge distribution in the adsorbent's molecular structure. When the pH level exceeds 7.4, as the pH of the solution rises, the positive charge on the DSAC@ZIF-8 (0.1:0.6) or solution interface reduces, and the adsorbent surface becomes negatively charged. Enhanced OH⁻ ions concentrations and ionic interaction between positively charged dye molecules and the positively charged surface, on the other hand, could explain higher adsorption at higher pH values. There are more exchangeable anions on the adsorbent's outer surface at higher pH values, resulting in improved adsorption. At a pH greater than pH_{pZC} where the surface is positively charged, cationic dye adsorption is more favourable [28].

3.2.2. Effect of dose

To determine the effect of adsorbent dosage, one of the most important parameters affecting adsorption, experiments were completed with solutions with an initial dye concentration. 1.9×10^{-3} mol/L and adsorbent dosage in the interval 0.01 to 0.25 g/25 mL. The experimental results are given in Fig. 8. The adsorption capacity of GV decreased as the dosage of the adsorbent increased due to unsaturated adsorption caused by insufficient adsorbate and excessive adsorbent. The more adsorbent adsorbed adsorbate resulted in decreased adsorption per unit mass of the adsorbent as the adsorbent dose increased, resulting in more unsaturated adsorption. Consequently, the adsorption potential decline [29–31].

3.2.3. Comparison between the different adsorbents

The effect of DSAC quantity on GV adsorption studies was studied. There was a comparison of DSAC, ZIF-8,

DSAC@ZIF-8 (0.05:0.6), and DSAC@ZIF-8 (0.1:0.6). The adsorbent dosage was 0.02 g; the dye solution volume was 25 mL, the concentration was 1.9×10^{-3} mol/L, the pH 9, and the shaking speed was 200 rpm. For DSAC@ZIF-8 (0.1:0.6), DSAC@ZIF-8 (0.05:0.6), ZIF-8, and DSAC, respectively, the efficiency of GV adsorption lowered from $1.56 > 1.52 > 1.49 > 1.47$ mmol/g (Fig. 9). Greater activated carbon produced from date seeds chemically activated with potassium hydroxide with increased microporosity for GV on DSAC@ZIF-8 (0.1:0.6) the best sample of adsorption as the amorphous increases, which is beneficial to dye adsorption operations, was linked to rising accessibility of receptors to magnified surface area for bulk adsorption of the dye [19,32]. Hence the adsorbent DSAC@ZIF-8 (0.1:0.6) was used in the experiments.

3.2.4. Effect of initial concentration

The effect of the initial concentration of tested dye GV on DSAC@ZIF-8 (0.1:0.6) was investigated at dye concentrations ranging from 2.76×10^{-4} to 2.2×10^{-3} mol/L

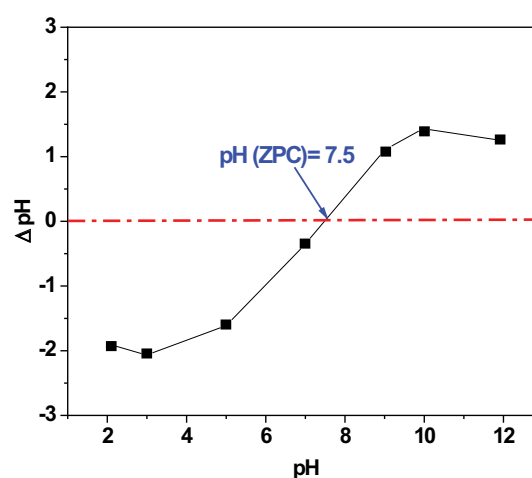


Fig. 6. The starting pH and the ΔpH of DSAC@ZIF-8 (0.1:0.6) are related.

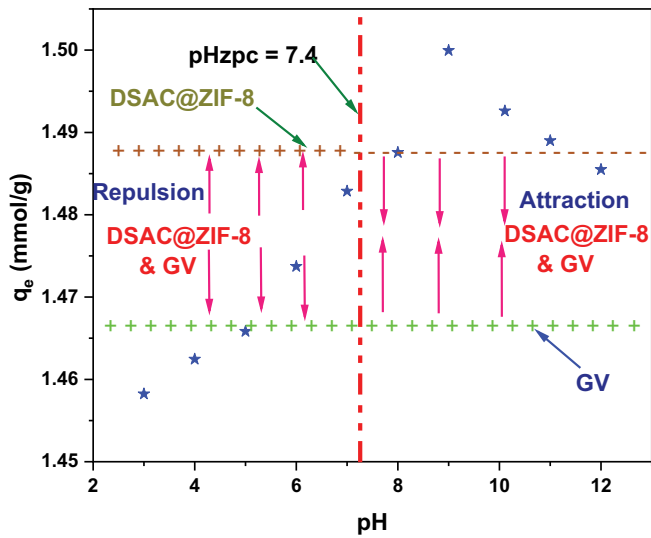


Fig. 7. The adsorbent (DSAC@ZIF-8) (0.1:0.6) has an impact on GV adsorption.

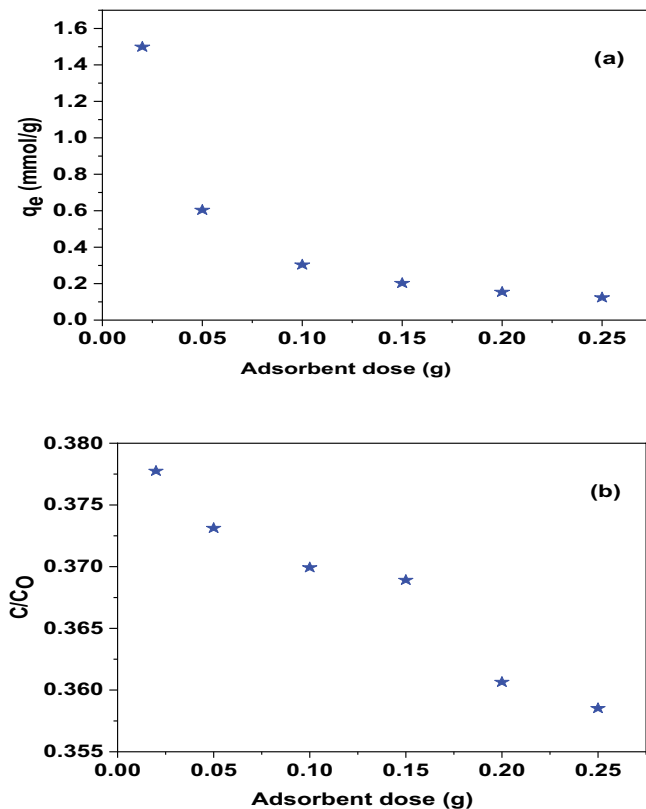


Fig. 8. Effect of DSAC@ZIF-8 (0.1:0.6) dosage on GV adsorption: (a) sorption capacity vs. DSAC@ZIF-8 (0.1:0.6) dose, (b) relative residual concentration (C/C_0) vs. DSAC@ZIF-8 (0.1:0.6) dose ($T: 25^\circ\text{C}; C_0: 1.9 \times 10^{-3} \text{ mol/L}$).

for GV at pH 9 and 0.02 g adsorbent. The percentage elimination declined as the initial dye concentration of GV increased. The percentage reduction in adsorption was due to binding the active binding sites of DSAC@ZIF-8 (0.1:0.6)

at higher concentrations with GV [33,34]. The greater DSAC@ZIF-8 (0.1:0.6) adsorption ability with increasing GV starting concentration could explain the increased interaction between the adsorbent and the dye (Fig. 10).

3.2.5. Adsorption isotherm

Langmuir [35,36], Freundlich [37], Temkin [38], Dubinin–Radushkevich [39] were used [Eqs. (3)–(6)]. The absorption of GV on DSAC@ZIF-8 (0.1:0.6) was considered using equilibrium isotherm models. The correlation coefficient (R^2) value's near to one was used to choose the best fit. The results of the isotherm modeling are summed up in this document (Table 3).

The Langmuir isotherm model seems to be the most accurate (Fig. 11). This indicates the presence of a monolayer adsorption process 1.579 mmol/g was the monolayer adsorption potential (q_m), 15.87 kJ/mol is the average sorption energy. In terms of the proposed chemisorption process, this is valid. The separation limit energy of 8 kJ/mol is universally acknowledged. Chemical sorption (up to 8 kJ/mol) and physical sorption (below 8 kJ/mol) are two different types of sorption [16].

$$\frac{C_e}{q_e} = \frac{1}{q_m K_L} + \frac{C_e}{q_m} \quad (\text{Langmuir}) \quad (3)$$

$$\ln q_e = \ln K_F + \frac{1}{n} \ln C_e \quad (\text{Freundlich}) \quad (4)$$

$$q_e = \beta_T \ln K_T + \beta_T \ln C_e \quad (\text{Temkin}) \quad (5)$$

$$\ln q_e = \ln Q_{DR} - K_{DR} \varepsilon^2 \quad (\text{Dubinin–Radushkevich}) \quad (6)$$

3.2.6. Adsorption kinetics and mechanism studies

The pseudo-first-order in this inquiry [41], pseudo-second-order [42], intraparticle was studied kinetically according to these models. The correlation coefficient (R^2) result getting as close to one as achievable was used to identify the best fit. An intraparticle mass transfer diffusion model was used because the pseudo-first-order and pseudo-second-order models failed to properly identify the governing diffusion process. Table 4 contains the findings of the kinetics modeling. Table 4 lists the pseudo-first-order constants (K_1) [Eq. (7)], pseudo-second-order constants (K_2) [Eq. (8)], and intraparticle diffusion rate constants [Eq. (9)]. Excellent properties, the pseudo-second-order is the best fit for the adsorption mechanism. The determination coefficient of $R^2 = 0.999$ is higher than the rest (R^2). This shows that adsorption kinetics are influenced by the availability of active sites and the amount of dye in the solution. The slope of the appropriate second linear area in the intraparticle diffusion kinetic model ($R^2 = 0.195$) for GV was determined (Fig. 12). The external barrier to mass transfer around the particles is only essential in the early stages of adsorption (initial sharp increase). The continuous adsorption with the intraparticle diffusion control approach is the second linear

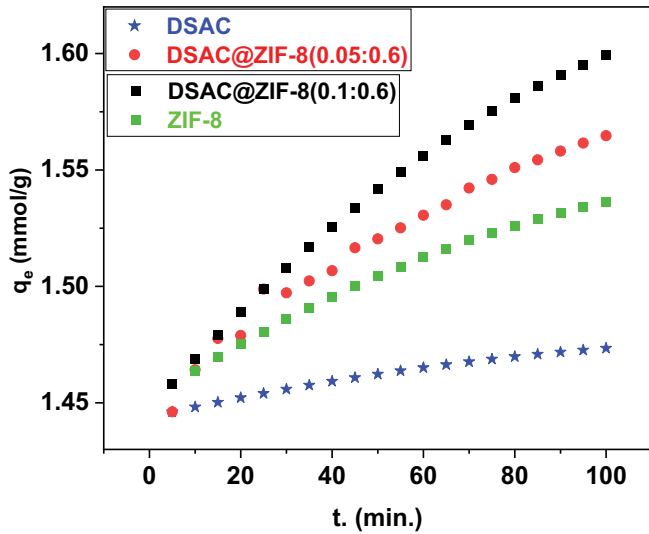


Fig. 9. Effect of different adsorbents DSAC, ZIF-8, DSAC@ZIF-8 (0.05:0.6), and DSAC@ZIF-8 (0.1:0.6) at adsorption of GV.

Table 3
For the adsorption of GV onto DSAC@ZIF-8 (0.1:0.6) nanoparticles, isotherms and their linear forms [40]

Isotherm	Value of parameters	
Langmuir	$q_{m,exp}$ (mmol/g)	1.5798
	q_m (mmol/g)	1.577
	K_L (L/mmol)	60,865.385
	R^2	0.9999
Freundlich	n	-1.2013
	K_F (mmol/g)(L/mmol) ^{1/n}	8.885
	R^2	0.77376
Dubinin–Radushkevich	Q_{DR}	1.178
	K_{DR} (J ² /mol ²)	-1.985E-09
	E_a (kJ/mol)	15.87
	R^2	0.8737
Temkin	b_T (L/mol)	11,605.1
	A_T (kJ/mol)	14.96
	R^2	0.92487

section. If the graphs do not cross through the origin, it means that pore diffusion isn't the only rate-limiting stage; alternative kinetic models, both of which can function simultaneously, can govern the adsorption rate.

$$\log(q_e - q_t) = \log q_e - \left(\frac{K_1}{2.303}\right)t \quad (7)$$

$$\frac{t}{q_t} = \frac{1}{K_2 q_e^2} + \frac{t}{q_e} \quad (8)$$

$$q_t = K_i t^{1/2} + X \quad (9)$$

Table 4
Kinetic parameters and their correlation coefficients for the adsorption of GV onto DSAC@ZIF-8 (0.1:0.6) nanoparticles [40]

Model	Value of parameters	
Pseudo-first-order kinetic	K_1 (min ⁻¹)	0.0144
	q_e (mmol/g)	0.128
	R^2	0.898
Pseudo-second-order kinetic	K_2 (g/mg min)	0.48087
	q_e (mmol/g)	1.575
	R^2	0.9998
Intraparticle diffusion	K_i (mg/g min ^{1/2})	-0.068
	X (mg/g)	0.55
	R^2	0.195
Elovich	β (g/mg)	-4.0816
	α (mg/g min)	2.7
	R^2	0.35
Experimental data	$q_{e,exp}$ (mmol/g)	1.565

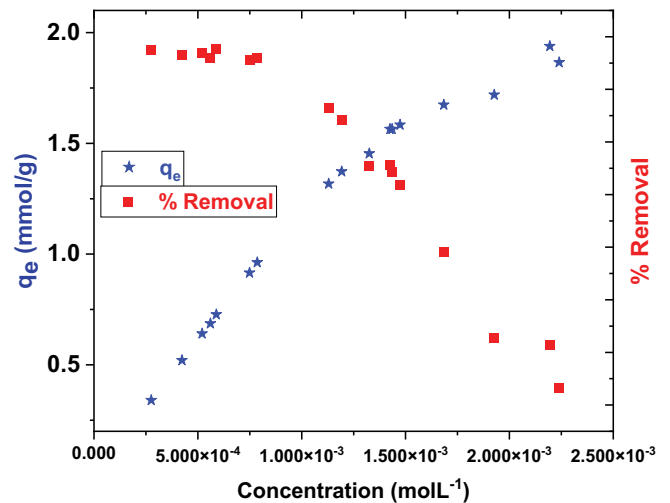


Fig. 10. Effect of initial dye concentrations on GV adsorption onto DSAC@ZIF-8 (0.1:0.6) (T : 25°C; C_0 : 2.76×10^{-4} to 2.2×10^{-3} mol/L).

The Elovich equation [Eq. (10)] predicts a wide range of chemisorption activation energies due to the heterogeneity of the adsorbent's active sites. The constant (related to the rate of chemisorption) increased as the dye concentration was increased, whereas the constant (related to the surface coverage) decreased (Table 4), this is due to a decrease in the adsorbate's usable adsorption surface. In conclusion, increasing the concentration within the studied range may speed up the chemisorption process. As an outcome, the adsorption kinetics may be satisfactorily approximated using the pseudo-second-order kinetic model. It is founded on the notion that rate-limiting chemisorption employs electrostatic forces, which involve the sharing or exchange of electrons between the adsorbent and the adsorbate [43,44].

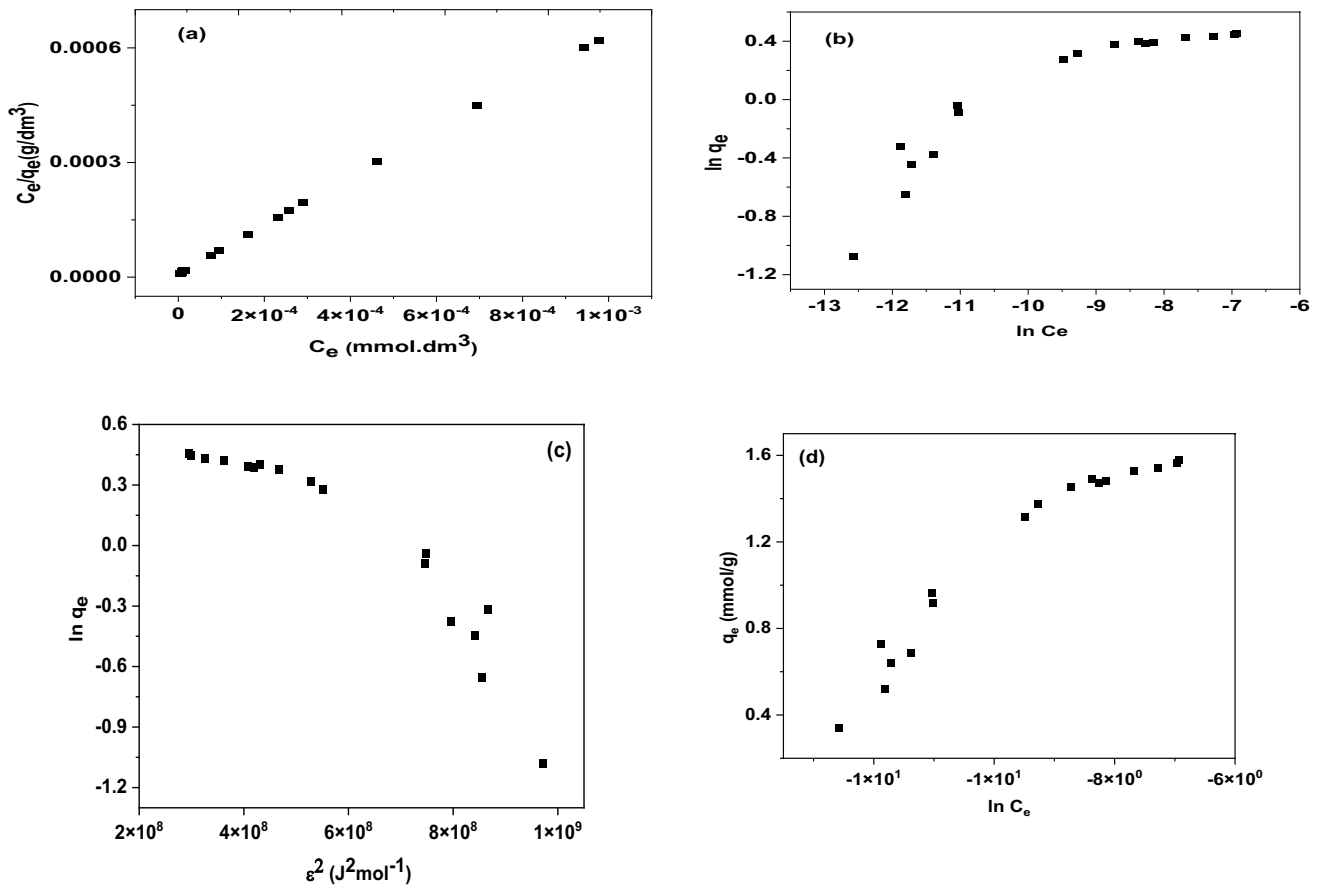


Fig. 11. (a) Langmuir, (b) Freundlich, (c) Dubin–Radushkevich, and (d) Temkin linearized isothermal sorption plots for GV (T : 25°C; C_0 : 2.76×10^{-4} to 2.2×10^{-3} mol/L).

$$q_t = \left(\frac{1}{\beta}\right) \ln(\alpha\beta) + \left(\frac{1}{\beta}\right) \ln t \quad (10)$$

On other hand, the adsorption of GV involves intraparticle diffusion and follows the pseudo-second-order kinetic model. DSAC@ZIF-8 (0.1:0.6) has high efficiency to remove GV, This may be due to the influence of the initial pH of the sorption solution on the surface properties of the sorbent and ionization–dissociation properties of the adsorbate molecule. Electrostatic interaction between the charged DSAC@ZIF-8 (0.1:0.6) surface and charged GV molecule may be considered as the principal adsorption mechanism. The adsorption isotherms of GV onto DSAC@ZIF-8 (0.1:0.6) were described by the Langmuir isotherm.

3.2.7. Studies on thermodynamic modeling

Investigate several aspects of DSAC@ZIF-8 (0.1:0.6) adsorptive elimination of GV, thermodynamics modeling was used to calculate (ΔG°), (ΔH°), and (ΔS°). Table 5 summarizes results at different temperatures of thermodynamic modeling Because of this, (ΔG°). If the value is

negative, the method is both possible and random [45,46]. At higher temperatures, the (ΔG°) values decreased from -9.7 to -18.2 kJ/mol, showing that GV elimination using DSAC@ZIF-8 (0.1:0.6) is becoming more beneficial. Gibbs' free energy transition ΔG° was found to be linear when plotted against temperature T (Fig. 13). (ΔH°) and (ΔS°) calculated 89.58 and 0.339 kJ/mol, respectively. An endothermic adsorption process is indicated by the presence of a positive (ΔH°) value. The existence of structural reforms on the adsorbent DSAC@ZIF-8 (0.1:0.6) during dye absorption is indicated by a positive value of (ΔS°), as the entropy increases the adsorption increase. The positive value of ΔS° also shows that the DSAC@ZIF-8 (0.1:0.6) adsorbent has a high affinity for GV [47,48].

The (ΔH°) and (ΔS°) of the adsorbed cycle were calculated using the slope and intercept of the $\ln K_c$ vs. $1/T$ plot, and E_a was calculated using the Arrhenius plot intercept (Fig. 14). In adsorption studies, the quantity of (ΔH°) is positive, indicating that the reaction is endothermic, while the value of (ΔG°) is negative, indicating that the reaction is spontaneous (Table 5 and Fig. 14). The fact that (ΔG°) became more negative as the temperature rose shows that "favorability" rises in tandem with the temperature [40,48]. In this situation, GV of the zero standard free energy temperature (T_0) is

predicted to be 264.3 K. The adsorbents tested are viable and can extract both colorants at very low temperatures, as seen by the low T_0 values.

1.569 mmol/g this mean when it converts to mg/g through multiplying with the molecular weight of GV it will be 638.99 mg/g.

3.3. Comparison with other adsorbents

Table 6 illustrates a comparison of maximal GV adsorption capacities employing DSAC@ZIF-8 (0.1:0.6) with other before-reported adsorbents. It indicates that the DSAC@ZIF-8 (0.1:0.6) is as expected has a high GV adsorption capability [49]. The maximum adsorption capacity was

3.4. Statistical and physical simulation

3.4.1. Models of adsorption

The use of a large canonical ensemble in statistical physics-based adsorption simulations allows for physical explanations derived from experimental conditions.

Table 5
For GV adsorption on DSAC@ZIF-8 (0.1:0.6), use (ΔG°), (ΔH°), and (ΔS°)

Dye	T (K)	ΔH° (kJ/mol)	ΔS° (J/mol K)	T_0 (K)	$-\Delta G^\circ$ (kJ/mol)
GV	298	89.58	338.97	264	9.7
	303				11.4
	308				13.11
	313				14.81
	318				18.19

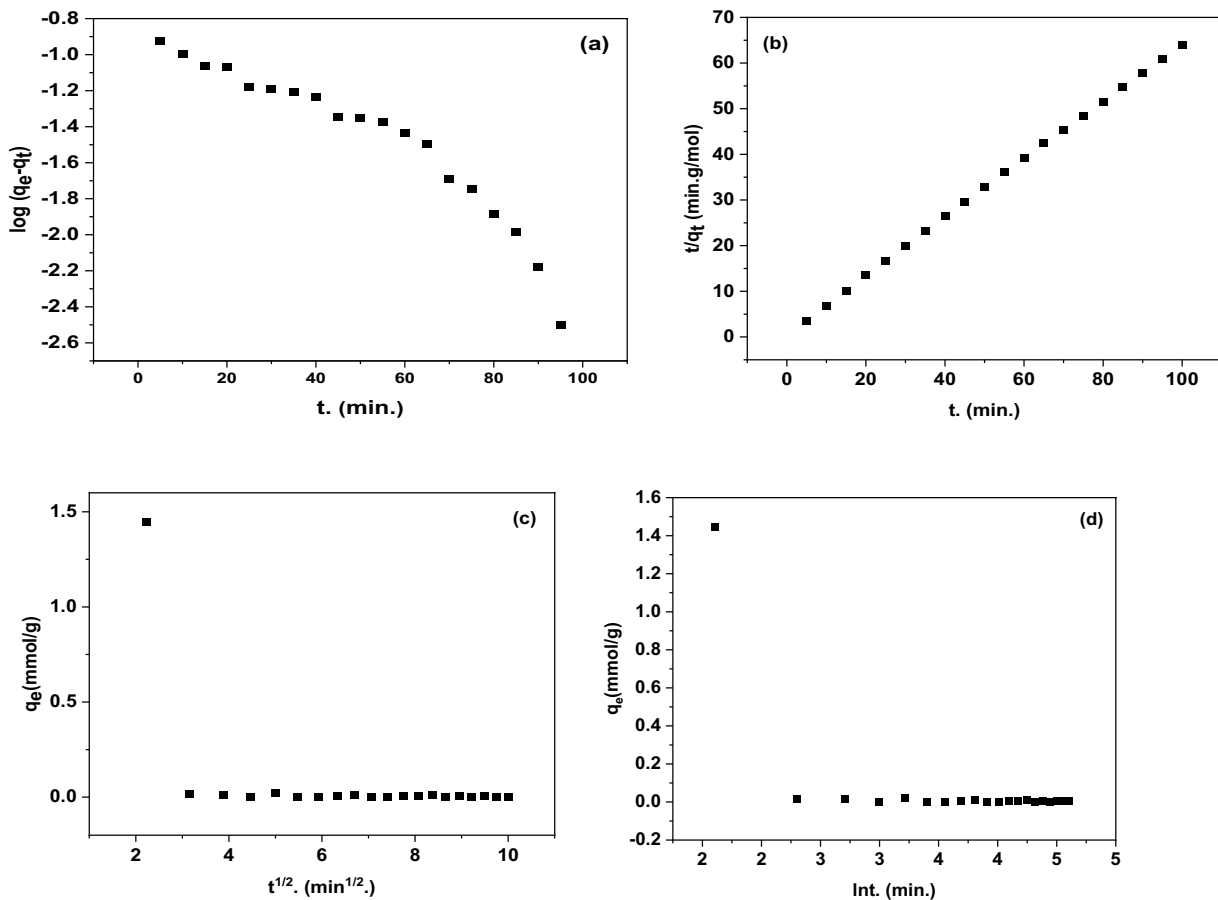


Fig. 12. Linearized kinetics study plots for GV: (a) pseudo-first-order, (b) pseudo-second-order, (c) intraparticle diffusion and (d) Elovich ($T: 25^\circ\text{C}$; $C_0: 1.9 \times 10^{-3}$ mol/L).

To accomplish this, some assumptions were made. First, the structure of an experimental isotherm, as determined by a statistical physics technique, influences the choice of the most effective ways to manage the isotherm model. The type of adsorption isotherm was determined using the IUPAC classification system. As a result, the first step is to choose the most suited model from the available possibilities. The model of monolayer adsorption coupled with ideal gas (MMIG) and the model of monolayer adsorption coupled with real gas (MMARG) was utilized in the current work for monolayer adsorption analysis (MMRG) [69]. The MMRG model considers the likelihood of adjacent contacts involving adsorbate molecules on the surface of an adsorbent; the MMIG model does not [70]. This hypothesis is especially relevant when it comes to how lateral interactions play a role in the adsorption process, specifically their impact just on the adsorption isotherm. The two models also think that, given a certain amount of energy, the adsorbate molecule can be multi-anchored or multi-molecularly adsorbed on the solid surface. To put it another way, both models allow for the determination of important steric and energetic variables that are important in the adsorption mechanism [70,71].

Adsorption isotherms, including Langmuir, describe adsorption on the surface of the adsorbent. The presence of monolayer adsorption over a wholly homogeneous surface with a fixed number of equal sites and minimal interaction between adsorbed molecules is related to the presence of monolayer adsorption over a completely homogeneous surface with a definite number of equal sites and minimal interaction between adsorbed molecules. The Freundlich model is an empirical equation based on adsorption of

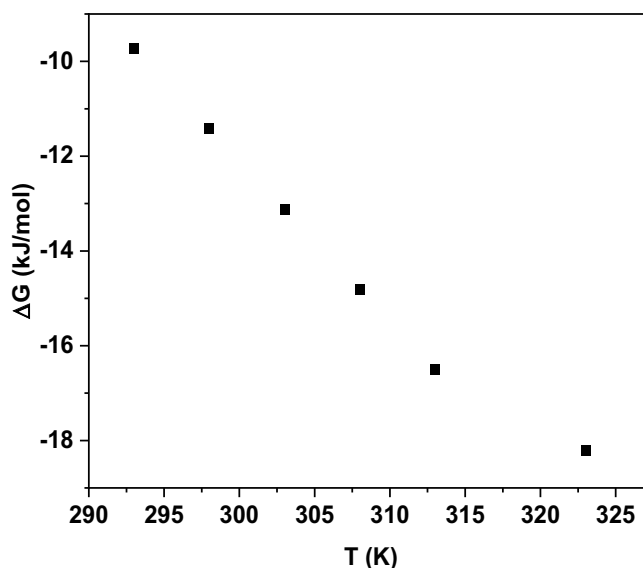


Fig. 13. The graph shows the change in Gibbs free energy (ΔG°) as a function of temperature (T) (T : 290–325 K; C_0 : 7.8×10^{-4} mol/L).

heterogeneous surface or surface supporting sites of varied affinities. It is assumed that the stronger binding sites are occupied first and that the binding strength decreases with the increasing degree of site occupation. The Dubinin–Radushkevich by determining the value of E , where E is the maximum energy which can be used to distinguish between physical (below 8 kJ/mol) and chemical (above 8 kJ/mol), and Temkin supposed that whenever the layer is covered,

Table 6
The GV dye adsorption capacity (q_m) of various adsorbents

Adsorbent	q_m (mg/g)	Reference
Fly ash	74.6	[50]
Bottom ash	12.1	[51]
Sulfuric acid	85.8	[52]
Activated carbon	19.8	[53]
ZFA zeolites from coal fly ash	19.6	[54]
Poly(acrylic acid-acrylamide-methacrylate)	35	[55]
Raw kaolin	26	[56]
Bagasse fly ash	79	[57]
Activated carbon	65	[58]
Activated carbon	175	[59]
Sewage sludge	263	[60]
Modified bentonite	457	[61]
Chitosan-g-(4-hydroxybenzoic acid)	18	[62]
Poly(vinyl benzyl chloride) beads	160	[63]
Ball clay	169	[64]
Magnetic κ -carrageenan beads	85	[65]
κ -carrageenan-poly(acrylic acid)/multi-walled carbon nanotube	118	[66]
Water hyacinth	32.28	[67]
Activated carbon 40°C	90.9	[68]
DSAC@ZIF-8 (0.1:0.6)	638.99	This work

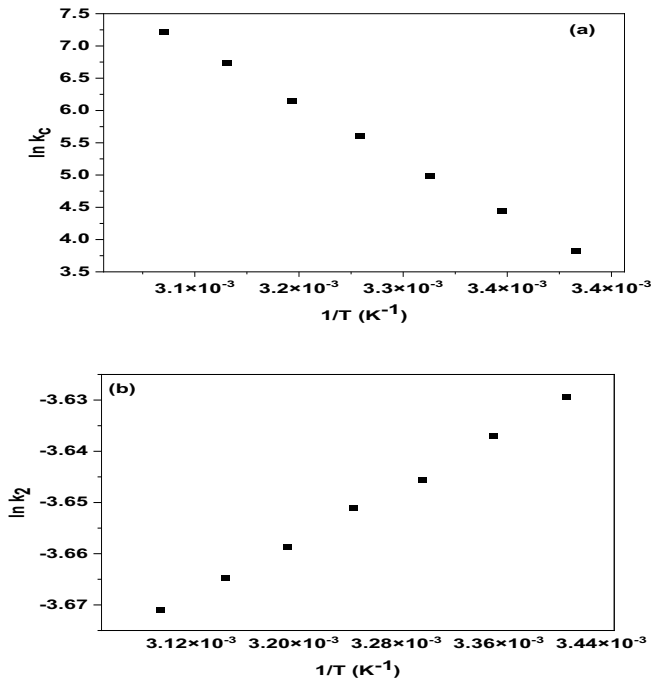


Fig. 14. (a) The adsorption of GV onto the DSAC@ZIF-8 (0.1:0.6) adsorbent is plotted by van't Hoff (T : 290:325 K; C_0 : 7.8×10^{-4} mol/L) and (b) For GV adsorption onto the DSAC@ZIF-8 (0.1:0.6), Arrhenius plots were used.

the heat of adsorption of all molecules drops linearly. The heat of adsorption of all molecules lowers linearly when the layer is covered.

It should also be mentioned that in the enhanced single layer model, the GV ions are deposited in a single adsorbed layer at the same energy level ($-E$). In the instance of double-layer ionic adsorption, we used a model that defines a double layer model. The alternate adsorption of

complimentary charge components in this circumstance results in the formation of two adsorbed layers. For this process to work, charge neutralization between GV cations and DSAC@ZIF-8 (0.1:0.6) anions is essential Table 7. The solid surface serves as a template at first, and then it is defunctionalized and employed as a fresh template for anionic ion adsorption after cationic ion adsorption [72,73].

To obtain the required model expressions, you must follow the steps:

Write the grand canonical partition feature [Eq. (11)] as follows:

$$Z_{gc} = \sum_{N_i} e^{-\beta(-\epsilon_i - \mu)N_i} \tag{11}$$

Determine the number of N_m receptors occupying similar locations [Eq. (12)]:

$$N_0 = \frac{1}{\beta} \frac{\sigma \ln(Z_{gc})^{N_m}}{\sigma \mu} \tag{12}$$

Calculate the adsorbed quantity, n [Eq. (13)]:

$$Q_m = n X N_0 \tag{13}$$

where μ is the chemical potential of the adsorbed phase, ($-\epsilon_i$) and N_i represents the adsorption energy and the occupation number of a receptor site i , respectively. $\beta = 1/k_B T$, where T is the absolute experimental temperature and k_B represents the Boltzmann's constant. Finally, n is the number or the fraction of the adsorbed molecule(s) per site.

For the designing and practical management of an adsorption system, the correlation of equilibrium data to theoretical equations is an essential procedure. The GV practical adsorption data on DSAC@ZIF-8 adsorbents is explained. Two models were utilized, both based on a statistical physics approach another method of putting

Table 7
The four isothermal models are represented analytically

Isotherm model	Adsorbed amount expression	Equation	Reference
MMIG	$Q_a = \frac{nN_m}{1 + \left(\frac{W}{c}\right)}$	(14)	[70]
MMRG	$Q_a = \frac{nN_m}{1 + \left(W \frac{1-bC}{C} e^{2\beta c} e^{-\frac{bC}{1-bC}}\right)^n}$	(15)	[69]
Double-layer model	$Q_a = Q_s \times \left(\frac{X_1 + 2X_2^2}{1 + X_1 + 2X_2^2}\right)$	(16)	[72]
Multi-layer model	$Q_a = Q_s \times \frac{X_1 + X_1 X_2 \left(1 - 2X_2^L - L X_2^{L+1} + \frac{X_2(1 - X_2^L)}{1 - X_2}\right)}{(1 - X_1)(1 - X_2) + X_1 X_2 (1 - X_2^L)}$	(17)	[74]

it, model of the models of monolayer adsorption coupled with ideal gas (MMIG) and monolayer adsorption coupled with real gas (MMRG) are two monolayer adsorption models (MMRG). The measured adsorption isotherms were modeled using the MMIG and MMRG models (Fig. 15). It must be noted that when the temperature increases, so do the GV adsorption potential of all of the adsorbents studied [75–77]. In respect of the models utilized, it could be demonstrated that they both closely match the experimental data. The fitting operation is non-linear, per the generalized reduced gradient algorithm, which was employed with the Microsoft Excel Solver Add-In. As a result, the model's evaluation. To establish the best fit, the extent of the correlation coefficient R^2 was utilized, as was universally acknowledged. Fitting experimental data with the model MMRG yielded the highest R^2 values (Table 8) [78]. In any event, the fitting precision differences supplied by the tested models are quite tiny, indicating poor departures from ideal gas behavior for the analyzed systems [79]. MMRG was therefore chosen as the most accurate model, supported by physical significance

and basic hypotheses. Indeed, In any case, the fitting precision differences provided by the tested models are fairly small, showing poor deviations to ideal gas performance for the subsystems under consideration. Adsorbate–adsorbate interactions must not be disregarded, as adsorbate molecules can attract or repelled adjacent molecules [71].

3.4.2. Description of statistical physics

A qualitative approach for identifying surface occurrences in adsorption is theoretical modeling of adsorption isotherms in the gas or liquid phase using a statistical physics method. The recovered model parameters are given a physical significance to have a better understanding of the reported adsorption events. As a result, Table 8 contains all of the MMIG and MMRG model's recoverable fitting parameters. In this sentence, the adsorption mechanisms are researched and then examined to describe and understand them. Table 9 shows that the pre-position number of adsorbed molecules, n , is less than the unit for DSAC@ZIF-8 at all temperatures examined. In terms of

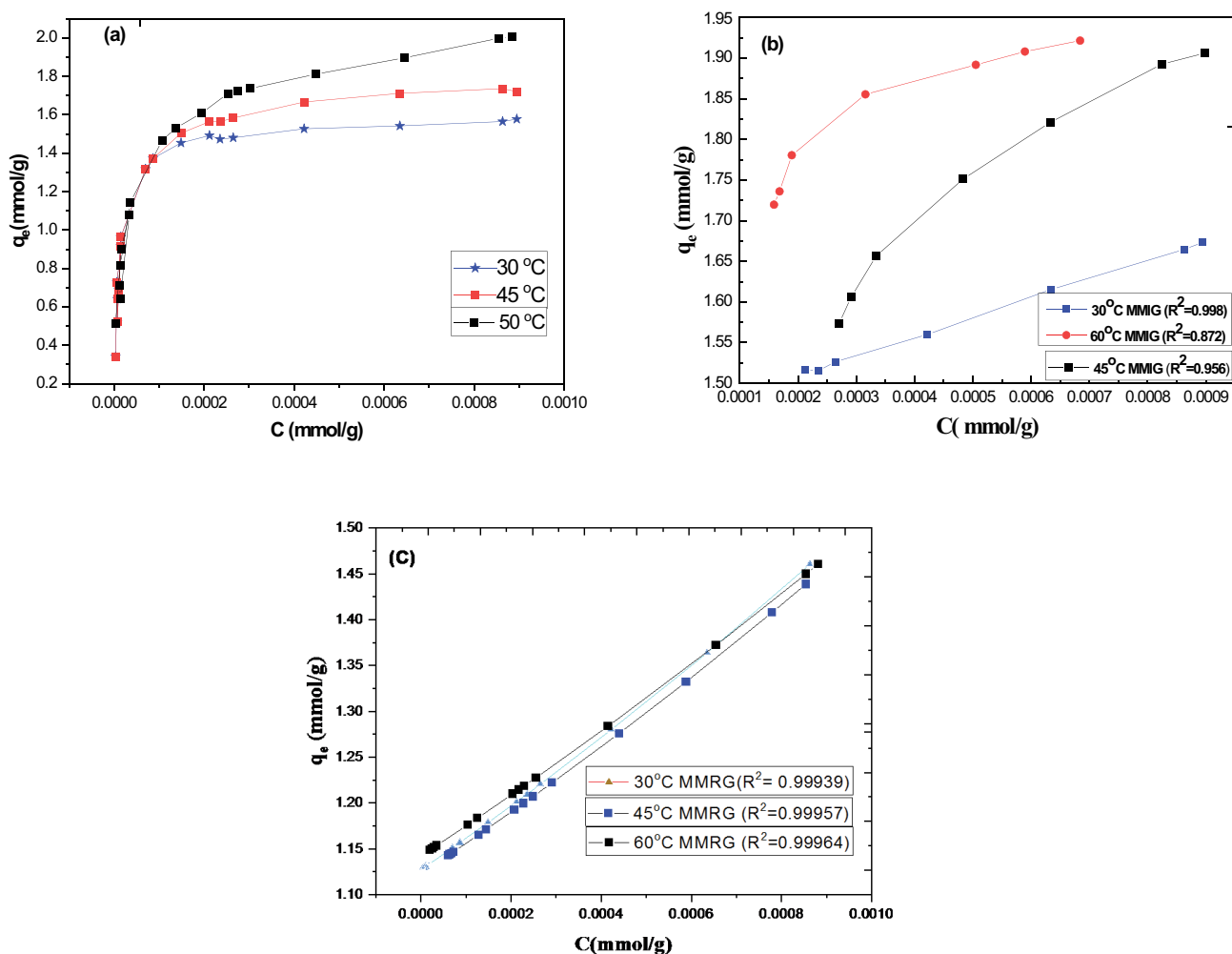


Fig. 15. Modeling of the Methylene blue practical adsorption isotherm with two variants of the adsorption isotherm in DSAC@ZIF-8 (0.1:0.6) (MMIG and MMRG).

the DSAC@ZIF-8 surface, this demonstrates that GV can indeed be adsorbed in DSAC@ZIF-8. Because of the electrostatic interactions between dye cations and nitrogen anions (N), we may extrapolate that GV could conceivably be adsorbed at numerous active sites on the DSAC@ZIF-8 surface via van der Waals forces or hydrogen bonding. In actuality, there was an agglomeration phenomenon when the energy of the surface increased (mainly due to the overlapping of potential fields of micropores walls), especially when it came to the temperature of adsorption increase. Furthermore, GV molecules form an aggregation in the solution either before or during adsorption. The density of receptor sites, N_m , is modified by temperature, as shown in Table 5. When comparing results at 30°C and 60°C adsorption temperatures, a larger number of receptor sites show. This is most likely due to adsorbate desolvation mechanisms and lower water adsorption, which is quickly replaced by GV molecules [78]. The specific concentration (w) reveals that DSAC@ZIF-8 has the maximum adsorption energy (lowest value of w), resulting in GV complete adsorption power (Table 9). The molecule's molecular pressure cohesion, a , and volume, b . As a result, these features are considered to have a small impact on the adsorption potential of the systems investigated. However, there is a slightly bigger volume value for GV adsorption at DSAC@ZIF-8 at 60°C, in this circumstance with the full potential of adsorption GV. Particularly in these settings, the attractive forces between adsorbed molecules are comparatively small (but not absent, as explained), as well as their mutual rivalry [71,75].

Parameters and their physical meaning

- n : Number of adsorbed molecules per site: This depicts the DSAC@ZIF-8 (0.1:0.6) surface position, as well as the adsorbed molecules during the adsorption process; adsorption can take place in either a vertical or horizontal multimolecular mechanism ($n > 1$), or ($n = 1$), through a parallel-oriented multi-anchored technique.
- The density of receptor sites (mg/g): Specifies the number of receptor sites that are successfully filled.

- w : The use of the equation above, estimate the adsorption intensity ($-E_a$) of GV on DSAC@ZIF-8 (0.1:0.6) from the dissolved state: $-E_a = RT \ln(w/C_s)$, where C_s (mg/L) is the soluble level and R (J/K mol) is the ideal gas constant.
- a (J L/mg): Molecular pressure cohesion: Due to the limited contact between adsorbed molecules and the strong adsorbent–adsorbate contacts, the development of this parameter is illustrated in a theoretical study; its drop is followed by a rise in the quantity of adsorbed materials.
- b (L/mg): Molecule volume: this factor has been proven to evolve in a theoretical investigation; the highest b value is followed by an increase in the adsorbed number. The attraction energy between adsorbed molecules becomes weak when the volume value is high [71].

3.4.3. Actual isotherms are adjusted using theoretical models

To determine the optimal statistical physics modeling that has a strong relationship with the empirical adsorption isotherms, we use computational software to correlate the experimental isotherms with the MMIG and MMRG models. The standard mathematical method for adapting experimental results with a given model is the Levenberg–Marquardt algorithm of iteration with a multivariate non-linear regression program.

Three error coefficients are used to compare the best-fitting model: The R^2 which evaluates the fit's suitability; the RMSE residual root mean square error; and the Akaike information criterion are the first three (AIC). Parameter values should be within ± 2 RMSE of their genuine values. Because the error coefficients obey the entry requirements, the MMIG and MMRG models were selected as measurement models for the adsorption of GV on DSAC@ZIF-8 (0.1:0.6) (the highest R^2 and the smallest RMSE and AIC). As just a result, we conclude that electrostatic interactions between the positively charged dye ion and the negatively charged DSAC@ZIF-8 (0.1:0.6) surface mediate GV adsorption. Cationic dyes are abbreviated as GV. In an aqueous solution,

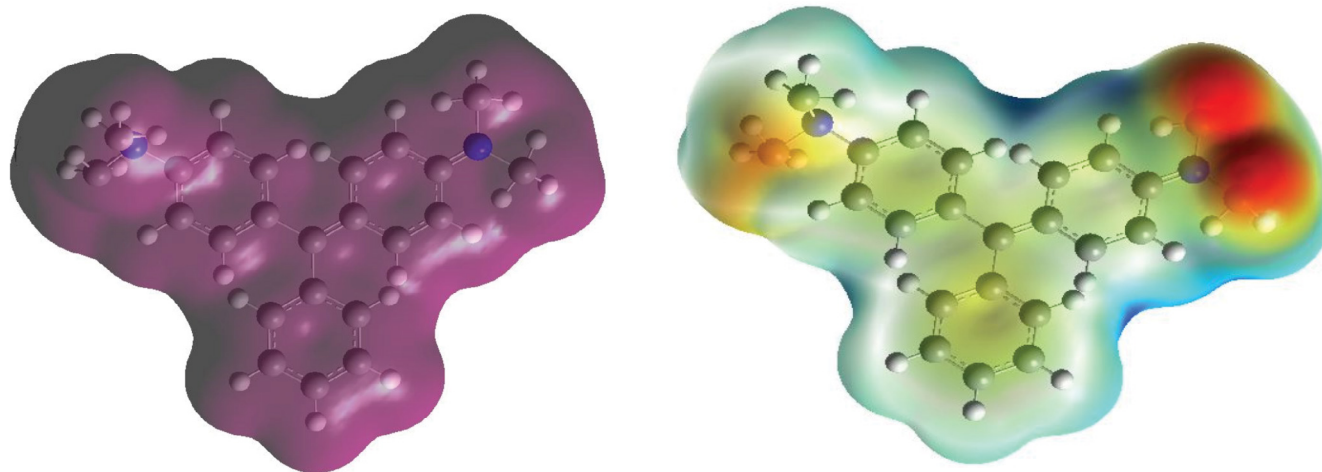


Fig. 16. Electron density molecular electrostatic potential (MEP) was used to map the whole electron density surface for GV.

Table 8
The evaluation coefficients of the MMIG and MMRG models are compared

Adsorbent	T (°C)	R ²		RMSE		AIC	
		MMIG	MMRG	MMIG	MMRG	MMIG	MMRG
DSAC@ZIF-8	30	0.998	0.9998	1.47	1.467	11.77	11.84
	45	0.872	0.99923	1.62	1.485	11.82	11.86
	60	0.956	0.99937	1.64	1.499	11.86	11.88

the dye dissociates into chloride anion (Cl⁻) and nitrogen ion (N⁺) [74].

3.5. Mechanism of interaction

The highest adsorption of GV was found to occur at pH greater than 7.5 (pH_{ZPC} of DSAC@ZIF-8 (0.1:0.6)). The development of surface hydrogen bonds between the hydroxyl groups on the DSAC@ZIF-8 surface and the nitrogen atoms of GV could explain this. On the DSAC@ZIF-8 surface, there are three potential orientations for GV adsorption:

- Only one of the amino groups is primarily engaged in surface bonding, resulting in charge localization.
- The GV's aromatic rings will be aligned perpendicular to the surface.
- The aromatic rings of the GV will be oriented horizontally to the surface in this orientation. The formation of a hydrogen bond or electrostatic contact generated by the resonance structure of GV are preferred methods of GV orientation in the horizontal plane.

The adsorption of GV, on the other hand, is based on intraparticle diffusion and follows a pseudo-second-order kinetic model. The effect of the initial pH of the sorption solution on the surface properties of the sorbent and the ionization–dissociation properties of the adsorbate molecule may explain why steam-processed activated carbons are so effective at removing GV. The main adsorption process could be electrostatic interaction between the charged DSAC surface and the charged GV molecule. The Langmuir isotherm was used to explain the adsorption isotherms of GV onto DSAC@ZIF-8.

Because the dye was cationic, when it was dissolved, it released colorful dye cations. When the pH was reduced from 9 to 2, the proportion of color removed dropped. It can be considered for two different dye adsorption mechanisms on the adsorbent: (i) an electrostatic contact between the dye molecule and the adsorbent; (ii) a chemical reaction between the dye and the adsorbent. The OH⁻ ion concentration increased at pH 9, and the adsorbent surface gained a negative charge by collecting OH⁻ ions. Because the charge at the adsorbent surface becomes negatively at high pH, there may be a strong electrostatic attraction between the negatively charged adsorbent surface and the cationic dye molecule, resulting in maximal dye adsorption.

The pH_{PZC} of DSAC@ZIF-8 was determined experimentally, and this composite has a pH_{ZPC} of 7.5. The number of negatively charged sites grows as the pH of the system rises, while the number of positively charged sites decreases. Due

Table 9
The variables of the MMRG model are fit at different temperatures for DSAC@ZIF-8 (0.1:0.6)

Parameter	T (°C)	DSAC@ZIF-8
<i>n</i>	30	5.9456
	45	6.011
	60	6.059
<i>N_m</i>	30	0.000726
	45	0.00057
	60	0.000614
<i>w</i>	30	1.717
	45	1.68
	60	1.66
<i>a</i> (J L/mg)	30	9.129 × 10 ⁻²⁰
	45	10.057 × 10 ⁻²⁰
	60	10.29 × 10 ⁻²⁰
<i>b</i> (L/mg)	30	0.416
	45	0.394
	60	0.38

to electrostatic attraction, negatively charged surface locations on the adsorbent surface favored adsorption. The presence of excess OH⁻ ions also causes greater adsorption of the selected cationic dye at alkaline pH.

3.6. Active sites

The approach of investigating the reactive sites in the tested adsorbate/adsorbents system and understanding the region of electrophilic/nucleophilic attack and the electrostatic potential zero regions is known as molecular electrostatic potential (MEP). In this study, the whole electron density surface of GV was mapped using MEP (Fig. 16). The varied values of the MEP were represented in these maps using different colors (red, yellow, green, light blue, and blue). Indeed, the negative values of the MEP were represented by red and yellow colors, which are associated with electrophilic assault; the positive values were represented by blue colors, which are associated with nucleophilic attack; and the MEP zero area was represented by green. The MEP of GV adsorbate indicates that the adsorbate is mostly prone to nucleophilic attack, as seen on the MEP map (Fig. 16). Furthermore, the MEP map reveals that the MEP approves that the GV adsorbate is mostly sensitive to nucleophilic assaults [71,80].

3.7. Desorption studies

The ability to regenerate and the stability of an adsorbent are two important aspects that affect its practical application. In three independent adsorption–desorption cycles, the adsorption potential of DSAC@ZIF-8 (0.1:0.6) has been investigated. The sorbent DSAC@ZIF-8 (0.1:0.6) was rinsed with distilled water after being cleaned with ethanol many times until colorless. The colorless DSAC@ZIF-8 (0.1:0.6) product was dried for 24 h at 60°C to get a consistent weight. The adsorbent is now ready for the second phase of absorption after regeneration. The regeneration efficiency of MG was determined to be 97.6%, 92.5%, and 90.6% for each adsorption/desorption cycle. After three cycles of testing, we employed XRD to examine the DSAC@ZIF-8 (0.1:0.6) material and determined that the crystallinity and structure were unchanged. The reusability of DSAC@ZIF-8 (0.1:0.6) nanoparticles is demonstrated in this study [19]. The following Eq. (18) was used to compute the regeneration efficiency:

$$\text{Regeneration efficiency (\%)} = \frac{\text{Total adsorption capacity in the second run}}{\text{Total adsorption capacity in the first run}} \times 100 \quad (18)$$

4. Conclusions

The functionalization of ZIF-8 with DSAC allows manufacturing a very efficient adsorbents of DSAC@ZIF-8 (0.05:0.6) and DSAC@ZIF-8 (0.1:0.6). The prepared adsorbents were characterized via FTIR, SEM, XRD and high surface area as BET surface area of 460.23 m²/g sorption capacities are 638.99 mg/g at pH 9 and 25°C of DSAC@ZIF-8 (0.1:0.6). The nature of the interaction between the dye cations and the adsorbent was found to be dependent upon the pH of the medium. The adsorption process carries out by a cation exchange mechanism; however, the adsorbent maintained a significant adsorption capacity at higher pH. The adsorption isotherms are well fitted by the Langmuir equation. Uptake kinetics is correctly fitted by the pseudo-second-order rate equation. The thermodynamic parameters have been determined: the reaction is endothermic, spontaneous. The randomness of the system increases with GV adsorption. A monolayer model coupled with the real gas law (MMRG) and a monolayer model linked with the ideal gas law (MMIG) were both investigated even under drastic conditions of high ionic strength, the sorbent maintained its high sorption capacity. The adsorption energy (E_a) of GV is 15 kJ/mol on average. It is advised that the chemisorption technique. The adsorbents can be used successfully up to 3 times without significant loss of its original efficiency regenerated by 1.0 M HCl. This means that the studied sorbent is a promising sorbent for the efficient removal of GV dye from wastewater of the textile industry.

Acknowledgements

The authors extend their appreciation to the Deanship of Scientific Research at King Khalid University for funding

this work through research groups program under Grant Number (R.G.P. 1/13/42).

References

- [1] M. Wakkal, B. Khiari, F. Zagrouba, Basic red 2 and methyl violet adsorption by date pits: adsorbent characterization, optimization by RSM and CCD, equilibrium and kinetic studies, *Environ. Sci. Pollut. Res.*, 26 (2019) 18942–18960.
- [2] N.P. Raval, P.U. Shah, N.K. Shah, Adsorptive amputation of hazardous azo dye Congo red from wastewater: a critical review, *Environ. Sci. Pollut. Res.*, 23 (2016) 14810–14853.
- [3] T.A. Saleh, Mercury sorption by silica/carbon nanotubes and silica/activated carbon: a comparison study, *J. Water Supply Res. Technol. AQUA*, 64 (2015) 892–903.
- [4] H. Hayzoun, A. Ouammou, O. Saidi, F. Khalil, L. Bouayyadi, Evaluation de la qualité bactériologique et chimique du Sebou, Maroc (Assessment of the bacteriological and chemical quality of the Sebou River, Morocco), *J. Mater. Environ. Sci.*, 5 (2014) 2438–2443.
- [5] N. Hassan, A. El-Sonbati, M.G. El-Desouky, Synthesis, characterization, molecular docking and DNA binding studies of Cu(II), Ni(II), Zn(II) and Mn(II) complexes, *J. Mol. Liq.*, 242 (2017) 293–307.
- [6] H.Ş. Aybar, F. Irani, M. Arslan, Performance analysis of single and double basin-inclined solar water distillation systems with and without black-fleece wick, *Desal. Water Treat.*, 57 (2016) 17167–17181.
- [7] L. Rozumová, O. Životský, J. Seidlerová, O. Motyka, I. Šafařík, M. Šafaříková, Magnetically modified peanut husks as an effective sorbent of heavy metals, *J. Environ. Chem. Eng.*, 4 (2016) 549–555.
- [8] M. Idrissi, Y. Miyah, Y. Benjelloun, M. Chaouch, Degradation of crystal violet by heterogeneous Fenton-like reaction using Fe/Clay catalyst with H₂O₂, *J. Mater. Environ. Sci.*, 7 (2016) 50–58.
- [9] M.G. El-Desouky, M. Abd El-Wahab, A.A. El-Bindary, Interpretations and DFT calculations for polypropylene/copper oxide nanosphere, *Biointerf. Res. Appl. Chem.*, 12 (2021) 1134–1147.
- [10] L. Ayed, K. Chaieb, A. Cheref, A. Bakhrouf, Biodegradation of triphenylmethane dye Malachite Green by *Sphingomonas paucimobilis*, *World J. Microbiol. Biotechnol.*, 25 (2009) 705–711.
- [11] D.A. Fungaro, C.P. Magdalena, Counterion effects on the adsorption of acid orange 8 from aqueous solution onto HDTMA-modified nanozeolite from fly ash, *Environ. Ecol. Res.*, 2 (2014) 97–106.
- [12] J. Wang, Z. Shi, J. Fan, Y. Ge, J. Yin, G. Hu, Self-assembly of graphene into three-dimensional structures promoted by natural phenolic acids, *J. Mater. Chem.*, 22 (2012) 22459–22466.
- [13] T. Ahmad, M. Danish, M. Rafatullah, A. Ghazali, O. Sulaiman, R. Hashim, M.N.M. Ibrahim, The use of date palm as a potential adsorbent for wastewater treatment: a review, *Environ. Sci. Pollut. Res.*, 19 (2012) 1464–1484.
- [14] Y. Feng, Y. Li, M. Xu, S. Liu, J. Yao, Fast adsorption of methyl blue on zeolitic imidazolate framework-8 and its adsorption mechanism, *RSC Adv.*, 6 (2016) 109608–109612.
- [15] F. Ke, Y.-P. Yuan, L.-G. Qiu, Y.-H. Shen, A.-J. Xie, J.-F. Zhu, X.-Y. Tian, L.-D.J. Zhang, Facile fabrication of magnetic metal-organic framework nanocomposites for potential targeted drug delivery, *J. Mater. Chem.*, 21 (2011) 3843–3848.
- [16] N. Hassan, A. Shahat, A. El-Didamony, M.G. El-Desouky, A.A. El-Bindary, Equilibrium, kinetic and thermodynamic studies of adsorption of cationic dyes from aqueous solution using ZIF-8, *Morocc. J. Chem.*, 8 (2020) 2627–2637.
- [17] T.A. Altalhi, M.M. Ibrahim, G.A.M. Mersal, M. Alsawat, M.H.H. Mahmoud, T. Kumeria, A. Shahat, M.A. El-Bindary, Mesopores silica nanotubes-based sensors for the highly selective and rapid detection of Fe²⁺ ions in wastewater, boiler system units and biological samples, *Anal. Chim. Acta*, 1180 (2021) 338860, doi: 10.1016/j.aca.2021.338860.

- [18] S.O. Badmus, T.A. Oyehan, T.A. Saleh, Enhanced efficiency of polyamide membranes by incorporating cyclodextrin-graphene oxide for water purification, *J. Mol. Liq.*, 340 (2021) 116991, doi: 10.1016/j.molliq.2021.116991.
- [19] N. Hassan, A. Shahat, A. El-Didamony, M.G. El-Desouky, A.A. El-Bindary, Synthesis and characterization of ZnO nanoparticles via zeolitic imidazolate framework-8 and its application for removal of dyes, *J. Mol. Struct.*, 1210 (2020) 128029, doi: 10.1016/j.molstruc.2020.128029.
- [20] A.A. El-Bindary, M.G. El-Desouky, M.A. El-Afiy, Thermal and spectroscopic studies of some prepared metal complexes and investigation of their potential anticancer and antiviral drug activity against SARS-CoV-2 by molecular docking simulation, *Biointerf. Res. Appl. Chem.*, 12 (2022) 1053–1075.
- [21] K. Yokota, M. Shimpo, T. Iwata, M. Hirose, T. Ikemoto, K.-i. Ohya, T. Katsuki, K. Shimada, K.J.I.M. Kario, A case of *Takayasu arteritis* with repeated coronary artery restenosis after drug-eluting stent implantation successfully treated with a combination of steroids, *Int. Med.*, 51 (2012) 739–743.
- [22] T.A. Saleh, The influence of treatment temperature on the acidity of MWCNT oxidized by HNO_3 or a mixture of $\text{HNO}_3/\text{H}_2\text{SO}_4$, *Appl. Surf. Sci.*, 257 (2011) 7746–7751.
- [23] N. Hassan, A. Shahat, A. El-Didamony, M.G. El-Desouky, A.A. El-Bindary, Mesoporous iron oxide nano spheres for capturing organic dyes from water sources, *J. Mol. Struct.*, 1217 (2020) 128361, doi: 10.1016/j.molstruc.2020.128361.
- [24] T.A. Saleh, Carbon nanotube-incorporated alumina as a support for MoNi catalysts for the efficient hydrodesulfurization of thiophenes, *Chem. Eng. J.*, 404 (2021) 126987, doi: 10.1016/j.cej.2020.126987.
- [25] T.A. Saleh, Protocols for synthesis of nanomaterials, polymers, and green materials as adsorbents for water treatment technologies, *Environ. Technol. Innov.*, 24 (2021) 101821, doi: 10.1016/j.eti.2021.101821.
- [26] A.S. Al-Wasidi, I.I. Al-Zahrani, H.I. Thawibaraka, A.M. Naglah, M.G. El-Desouky, M.A. El-Bindary, Adsorption studies of carbon dioxide and anionic dye on green adsorbent, *J. Mol. Struct.*, 1250 (2021) 131736, doi: 10.1016/j.molstruc.2021.131736.
- [27] T.A. Saleh, Isotherm, kinetic, and thermodynamic studies on Hg (II) adsorption from aqueous solution by silica-multiwall carbon nanotubes, *Environ. Sci. Pollut. Res.*, 22 (2015) 16721–16731.
- [28] M. Özacar, İ.A. Şengil, Adsorption of reactive dyes on calcined alunite from aqueous solutions, *J. Hazard. Mater.*, 98 (2003) 211–224.
- [29] C. Djalani, R. Zaghdoudi, F. Djazi, B. Boucekima, A. Lallam, A. Modarressi, M. Rogalski, Adsorption of dyes on activated carbon prepared from apricot stones and commercial activated carbon, *J. Taiwan Inst. Chem. Eng.*, 53 (2015) 112–121.
- [30] T.A. Saleh, A.M. Elsharif, O.A. Bin-Dahman, Synthesis of amine functionalization carbon nanotube-low symmetry porphyrin derivatives conjugates toward dye and metal ions removal, *J. Mol. Liq.*, 340 (2021) 117024, doi: 10.1016/j.molliq.2021.117024.
- [31] G.A.A. AlHazmi, K.S. AbouMelha, M.G. El-Desouky, A.A. El-Bindary, Effective adsorption of doxorubicin hydrochloride on zirconium metal-organic framework: equilibrium, kinetic and thermodynamic studies, *J. Mol. Struct.*, 1258 (2022) 132679, doi: 10.1016/j.molstruc.2022.132679.
- [32] T.A. Saleh, Trends in the sample preparation and analysis of nanomaterials as environmental contaminants, *Trends Environ. Anal. Chem.*, 28 (2020) e00101, doi: 10.1016/j.teac.2020.e00101.
- [33] S. Wong, N.A.N. Yac'cob, N. Ngadi, O. Hassan, I.M. Inuwa, From pollutant to solution of wastewater pollution: Synthesis of activated carbon from textile sludge for dye adsorption, *Chin. J. Chem. Eng.*, 26 (2018) 870–878.
- [34] T.A. Saleh, Characterization, determination and elimination technologies for sulfur from petroleum: toward cleaner fuel and a safe environment, *Trends Environ. Anal. Chem.*, 25 (2020) e00080, doi: 10.1016/j.teac.2020.e00080.
- [35] I. Langmuir, The constitution and fundamental properties of solids and liquids. II. Liquids, *J. Am. Chem. Soc.*, 39 (1917) 1848–1906.
- [36] I. Langmuir, The adsorption of gases on plane surfaces of glass, mica and platinum, *J. Am. Chem. Soc.*, 40 (1918) 1361–1403.
- [37] H. Freundlich, W. Heller, The adsorption of cis-and trans-azobenzene, *J. Am. Chem. Soc.*, 61 (1939) 2228–2230.
- [38] R. Rezaei, M. Massinaei, A.Z. Moghaddam, Removal of the residual xanthate from flotation plant tailings using modified bentonite, *Miner. Eng.*, 119 (2018) 1–10.
- [39] M. Dubinin, Sorbtsiya I Struktura Aktivnykh Uglei 1. Issledovanie Adsorbtsii Organicheskikh Parov, *Zh. Fizich. Khim.*, 21 (1947) 1351–1362.
- [40] M.A. El-Bindary, M.G. El-Desouky, A.A. El-Bindary, Adsorption of industrial dye from aqueous solutions onto thermally treated green adsorbent: a complete batch system evaluation, *J. Mol. Liq.*, 346 (2022) 117082, doi: 10.1016/j.molliq.2021.117082.
- [41] S.K. Lagergren, About the theory of so-called adsorption of soluble substances, *Kungl. Svens. Vetenskapsakad. Handl.*, 24 (1898) 1–39.
- [42] Y.-S. Ho, G. McKay, Sorption of dye from aqueous solution by peat, *Chem. Eng. J.*, 70 (1998) 115–124.
- [43] M.G. El-Desouky, A. Shahat, A.A. El-Bindary, M.A. El-Bindary, Description, kinetic and equilibrium studies of the adsorption of carbon dioxide in mesoporous iron oxide nanospheres, *Biointerf. Res. Appl. Chem.*, 12 (2022) 1022–1038.
- [44] H.A. Kiwaan, T.M. Atwee, E.A. Azab, A.A. El-Bindary, Efficient photocatalytic degradation of Acid Red 57 using synthesized ZnO nanowires, *J. Chin. Chem. Soc.*, 66 (2019) 89–98.
- [45] R. Juang, F. Wu, R. Tseng, The ability of activated clay for the adsorption of dyes from aqueous solutions, *Environ. Technol.*, 18 (1997) 525–531.
- [46] H. Nollet, M. Roels, P. Lutgen, P. Van der Meeren, W. Verstraete, Removal of PCBs from wastewater using fly ash, *Chemosphere*, 53 (2003) 655–665.
- [47] M. Fathi, A. Asfaram, A. Farhangi, Removal of Direct Red 23 from aqueous solution using corn stalks: isotherms, kinetics and thermodynamic studies, *Spectrochim. Acta A*, 135 (2015) 364–372.
- [48] C. Prasad, S. Karlapudi, P. Venkateswarlu, I. Bahadur, S. Kumar, Green arbitrated synthesis of Fe_3O_4 magnetic nanoparticles with nanorod structure from pomegranate leaves and Congo red dye degradation studies for water treatment, *J. Mol. Liq.*, 240 (2017) 322–328.
- [49] M. El-Desouky, M.A. El-Bindary, A.A. El-Bindary, Effective adsorptive removal of anionic dyes from aqueous solution, *Vietn. J. Chem.*, 59 (2021) 341–361.
- [50] E. Eren, O. Cubuk, H. Ciftci, B. Eren, B. Caglar, Adsorption of basic dye from aqueous solutions by modified sepiolite: equilibrium, kinetics and thermodynamics study, *Desalination*, 252 (2010) 88–96.
- [51] K.Z. Elwakeel, A.A. El-Bindary, E.Y. Kouta, Retention of copper, cadmium and lead from water by Na-Y-Zeolite confined in methyl methacrylate shell, *J. Environ. Chem. Eng.*, 5 (2017) 3698–3710.
- [52] Y. Lin, X. He, G. Han, Q. Tian, W. Hu, Removal of Crystal Violet from aqueous solution using powdered mycelial biomass of *Ceriporia lacerata* P2, *J. Environ. Sci.*, 23 (2011) 2055–2062.
- [53] N.J. Vickers, Animal communication: when i'm calling you, will you answer too?, *Curr. Biol.*, 27 (2017) R713–R715.
- [54] H.A. Kiwaan, F.Sh. Mohamed, A.A. El-Bindary, N.A. El-Ghamaz, H.R. Abo-Yassin, M.A. El-Bindary, Synthesis, identification and application of metal organic framework for removal of industrial cationic dyes, *J. Mol. Liq.*, 342 (2021) 117435, doi: 10.1016/j.molliq.2021.117435.
- [55] S. Li, Removal of crystal violet from aqueous solution by sorption into semi-interpenetrated networks hydrogels constituted of poly (acrylic acid-acrylamide-methacrylate) and amylose, *Bioresour. Technol.*, 101 (2010) 2197–2202.
- [56] C. Puri, G. Sumana, Highly effective adsorption of crystal violet dye from contaminated water using graphene oxide intercalated montmorillonite nanocomposite, *Appl. Clay Sci.*, 166 (2018) 102–112.
- [57] I.D. Mall, V.C. Srivastava, N.K. Agarwal, Removal of Orange-G and Methyl Violet dyes by adsorption onto bagasse fly

- ash—kinetic study and equilibrium isotherm analyses, *Dyes Pigm.*, 69 (2006) 210–223.
- [58] K. Mohanty, J.T. Naidu, B. Meikap, M. Biswas, Removal of crystal violet from wastewater by activated carbons prepared from rice husk, *Ind. Eng. Chem. Res.*, 45 (2006) 5165–5171.
- [59] S. Wang, Z. Zhu, Effects of acidic treatment of activated carbons on dye adsorption, *Dyes Pigm.*, 75 (2007) 306–314.
- [60] M. Otero, F. Rozada, L. Calvo, A. Garcia, A. Moran, Elimination of organic water pollutants using adsorbents obtained from sewage sludge, *Dyes Pigm.*, 57 (2003) 55–65.
- [61] E. Eren, Removal of basic dye by modified Unye bentonite, Turkey, *J. Hazard. Mater.*, 162 (2009) 1355–1363.
- [62] A.-C. Chao, S.-S. Shyu, Y.-C. Lin, F.-L. Mi, Enzymatic grafting of carboxyl groups on to chitosan to confer on chitosan the property of a cationic dye adsorbent, *Bioresour. Technol.*, 91 (2004) 157–162.
- [63] D. Kaner, A. Saraç, B.F. Şenkal, Removal of dyes from water using crosslinked aminomethane sulfonic acid based resin, *Environ. Geochem. Health*, 32 (2010) 321–325.
- [64] P. Monash, R. Niwas, G. Pugazhenth, Utilization of ball clay adsorbents for the removal of crystal violet dye from aqueous solution, *Clean Technol. Environ. Policy*, 13 (2011) 141–151.
- [65] G.R. Mahdavinia, S. Iravani, S. Zoroufi, H. Hosseinzadeh, Magnetic and K⁺-cross-linked kappa-carrageenan nanocomposite beads and adsorption of crystal violet, *Iran. Polym. J.*, 23 (2014) 335–344.
- [66] H. Hosseinzadeh, Synthesis of carrageenan/multi-walled carbon nanotube hybrid hydrogel nanocomposite for adsorption of crystal violet from aqueous solution, *Pol. J. Chem. Technol.*, 17 (2015) 70–76.
- [67] M.R. Kulkarni, T. Revanth, A. Acharya, P. Bhat, Removal of Crystal Violet dye from aqueous solution using water hyacinth: equilibrium, kinetics and thermodynamics study, *Res.-Eff. Technol.*, 3 (2017) 71–77.
- [68] M. Abbas, Z. Harrache, M. Trari, Removal of Gentian violet in aqueous solution by activated carbon equilibrium, kinetics, and thermodynamic study, *Adsorpt. Sci. Technol.*, 37 (2019) 566–589.
- [69] A. Nakhli, M. Bergaoui, M. Khalfaoui, J. Möllmer, A. Möller, A.B. Lamine, Modeling of high pressure adsorption isotherm using statistical physics approach: lateral interaction of gases adsorption onto metal–organic framework HKUST-1, *Adsorption*, 20 (2014) 987–997.
- [70] M. Khalfaoui, S. Knani, M. Hachicha, A.B. Lamine, New theoretical expressions for the five adsorption type isotherms classified by BET based on statistical physics treatment, *J. Colloid Interface Sci.*, 263 (2003) 350–356.
- [71] A. Nakhli, M. Bergaoui, K.H. Toumi, M. Khalfaoui, Y. Benguerba, M. Balsamo, F.E. Soetaredjo, S. Ismadji, B. Ernst, A. Erto, Molecular insights through computational modeling of methylene blue adsorption onto low-cost adsorbents derived from natural materials: a multi-model's approach, *Comput. Chem. Eng.*, 140 (2020) 106965, doi: 10.1016/j.compchemeng.2020.106965.
- [72] M.B. Yahia, M.B. Yahia, New insights in the physicochemical investigation of the vitamin B 12 nucleus using statistical physics treatment: interpretation of experiments and surface properties, *RSC Adv.*, 10 (2020) 21724–21735.
- [73] A.Q. Al-Gamal, W.S. Falath, T.A. Saleh, Enhanced efficiency of polyamide membranes by incorporating TiO₂-Graphene oxide for water purification, *J. Mol. Liq.*, 323 (2021) 114922, doi: 10.1016/j.molliq.2020.114922.
- [74] M.B. Yahia, F. Aouaini, M.B. Yahia, E.S. Almogait, H. Al-Ghamdi, Theoretical investigation of the chlorophyll nucleus adsorption monitored with Quartz Crystal Microbalance technique: new insights on physicochemical properties, *J. Mol. Liq.*, 289 (2019) 111188, doi: 10.1016/j.molliq.2019.111188.
- [75] M. Khalfaoui, M. Baouab, R. Gauthier, A.B. Lamine, Acid dye adsorption onto cationized polyamide fibres. Modeling and consequent interpretations of model parameter behaviours, *J. Colloid Interfaces Sci.*, 296 (2006) 419–427.
- [76] N. Hassan, A. Shahat, I.M. El-Deen, M.A.M. El-Afify, M.A. El-Bindary, Synthesis and characterization of NH₂-MIL-88(Fe) for efficient adsorption of dyes, *J. Mol. Struct.*, 1258 (2022) 132662, doi: 10.1016/j.molstruc.2022.132662.
- [77] H.A. Kiwaan, F.Sh. Mohamed, N.A. El-Ghamaz, N.M. Beshry, A.A. El-Bindary, Experimental and electrical studies of Na-X zeolite for the adsorption of different dyes, *J. Mol. Liq.*, 332 (2021) 115877, doi: 10.1016/j.molliq.2021.115877.
- [78] O.V. Ovchinnikov, A.V. Evtukhova, T.S. Kondratenko, M.S. Smirnov, V.Yu. Khokhlov, O.V. Erina, Manifestation of intermolecular interactions in FTIR spectra of methylene blue molecules, *Vib. Spectrosc.*, 86 (2016) 181–189.
- [79] A.B. Lamine, Y. Bouazra, Application of statistical thermodynamics to the olfaction mechanism, *Chem. Senses*, 22 (1997) 67–75.
- [80] A.S. Al-Wasidi, I.I.S. AlZahrani, A.M. Naglah, M.G. El-Desouky, M.A. Khalil, A.A. El-Bindary, M.A. El-Bindary, Effective removal of Methylene Blue from aqueous solution using metal–organic framework; modelling analysis, statistical physics treatment and DFT calculations, *ChemistrySelect*, 6 (2021) 11431–11447.